Chaos-induced resistivity in the magnetic null region: A nonlinear mechanism of collisionless dissipation

Ryusuke Numata* and Zensho Yoshida†
Graduate School of Frontier Sciences, University of Tokyo, Hongo, Tokyo 113-0033, Japan
(Received 10 January 2003; published 14 July 2003)

Magnetic null points act as scattering centers where particles describe chaotic orbits, and the mixing effect brings about increase of the kinetic entropy. The resultant ''chaos-induced resistivity'' may explain anomalous diffusion of current in magnetic null regions [Phys. Rev. Lett. **88**, 045003 (2002)], which can be much larger than the conventional collisionless resistivity in a high temperature plasma. To study the statistical properties of the system (such as Lyapunov exponents and distribution functions), strong spatial inhomogeneity of the system has been studied to specify the responsible ''chaos region.''

DOI: 10.1103/PhysRevE.68.016407 PACS number(s): 52.20.Dq, 05.45.−a, 96.60.Rd

I. INTRODUCTION

Spatial variations of electromagnetic fields yield nonlinearity in charged particle dynamics. Chaotic motion of particles is an important mechanism of producing resistivity in an almost collisionless plasma [1–3]. A strongly inhomogeneous magnetic field including null points breaks the conservation of adiabatic invariants. The increase of the degree of freedom can result in chaotic motion of particles. The mixing effect of chaos brings about rapid increase of the kinetic entropy in a collisionless plasma, which, however, is not sufficient to yield a diffusion-type dissipation. When a test particle is confined in a bounded domain of the phase space, the second cumulant of the velocity distribution saturates after the initial mixing phase, and hence the diffusion constant (the time derivative of the second cumulant) diminishes to zero. However, in an open system where particles can convect into or out a chaotic region of the phase space (either through coordinate or momentum axes), particles are heated locally during a certain staying time in the chaos region, and a continuous dissipation process is achieved there [3].

In this paper, we study the motion of particles in a Y-shape magnetic field with perpendicular electric field (Fig. 1). If particles are far from the magnetic null point, they are magnetized and describe ordered $\boldsymbol{E}\times\boldsymbol{B}$ drift orbits. However, motion of particles becomes chaotic in a certain neighborhood of the null point. By analyzing motion of many particles (we consider independent particles ignoring collisions), we observe collisionless heating of particles in the chaos region. This is in marked contrast to the motion of magnetized particles that cannot gain energy from a stationary electric field because of the periodicity of motion. Evaluating the average velocity of particles in the direction parallel to the electric field, we may estimate the effective collisionless resistivity.

This theory may be applied to various collisionless magnetic diffusion phenomena, especially to fast magnetic reconnections leading to changes of magnetic topologies [1–6]. Tearing modes in tokamaks, magnetic substorms or solar flares are significantly accelerated by ''anomalous resistivities.'' Wave-particle interactions (through lower hybrid drift instabilities) [4] or stochasticity of magnetic field lines [5] have been studied to account for enhanced resistivities. The collisionless resistivity studied here stems from microscopic particle dynamics that cannot be studied by a fluid model or the Vlasov equation. We consider magnetic null points that unmagnetize particles and cause a highly nonintegrable motion. The resultant rapid entropy production may be applied to overcome the difficulty of the Petschek model of magnetic reconnections [6].

The standard normalization of Newton's equation of motion shows that the particle inertial effect (kinetic effect) works in a length scale of the skin depth (Sec. II). Single-particle motion is analyzed in Sec. III. We introduce an ensemble-averaged ''local Lyapunov exponent,'' and specify the ''chaos region.'' The spatial inhomogeneity of the system is essential—the randomization of orbits and the resultant resistivity are strongly localized in the neighborhoods of null

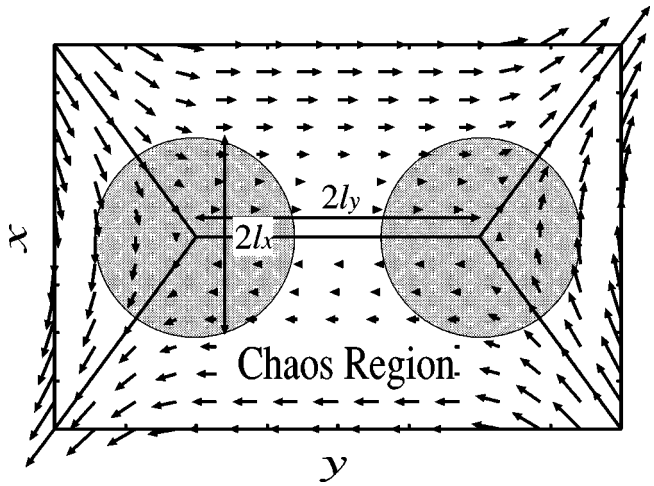

FIG. 1. A Y-shape magnetic field with $\ell\equiv\ell_y/\ell_x=2$ projected onto the x-y plane. (x and y coordinates are normalized to the system size ℓ_x.) The chaos region (hatched region) is defined by using the local Lyapunov exponents in Sec. III B.

*Electronic address: numata@plasma.q.t.u-tokyo.ac.jp
†Electronic address: yoshida@k.u-tokyo.ac.jp

points. Particle convection connects the chaos region and the outside regular region, and hence the chaos region (not *a priori* determined) must be treated as an open system. In Sec. IV, we study the statistical distribution of chaotic particles. The chaos-induced resistivity is scaled by the Alfvén Mach number, while it does not depend on plasma temperature. In high temperature plasmas, such as, solar corona, the present chaos-induced resistivity is much higher than the classical collisional resistivity.

II. MODEL EQUATION

We consider a two-dimensional Y-shape (and X-shape magnetic field as the degenerate case) magnetic field (Fig. 1), which can be written as (in Cartesian coordinates)

$$\boldsymbol{B}=\begin{cases}(B_0(y\mp\ell_y)/\ell_x, B_0 x/\ell_x, 0) & (|y|>\ell_y)\\ (0, B_0 x/\ell_x, 0) & (|y|\leqslant\ell_y),\end{cases} \tag{1}$$

where B_0, ℓ_x, and ℓ_y are constant numbers. The plane of $x=0, |y|\leqslant\ell_y$ is called a neutral sheet where the magnetic field vanishes. We apply a constant electric field in the direction perpendicular to the magnetic field:

$$\boldsymbol{E}=E_0\boldsymbol{e}_z=-\boldsymbol{\nabla}\phi, \tag{2}$$

where E_0 is a constant, $\boldsymbol{e}_z=\boldsymbol{\nabla}z$, and ϕ is the electrostatic potential. The potentials are given by

$$A_z(x,y)=\begin{cases}\dfrac{B_0}{2\ell_x}[(y\mp\ell_y)^2-x^2] & (|y|>\ell_y)\\ -\dfrac{B_0}{2\ell_x}x^2 & (|y|\leqslant\ell_y),\end{cases}$$

$$\phi(z)=-E_0 z. \tag{3}$$

The Hamiltonian of a single particle includes all three coordinates, so that the orbit is generally nonintegrable (chaotic) [7]. In the neighborhood of the Y points, particles describe chaotic orbits receiving almost random sequences of acceleration and deceleration from the electric field. As we will show later, the resultant randomization of orbits yields a collisionless resistivity. On the other hand, outside this chaos region (to be specified more quantitatively in Sec. III B), the magnetic field is sufficiently strong to magnetize particles (the magnetic moment $\mu\equiv mv_\perp^2/2B$ conserves), and the guiding centers describe $\boldsymbol{E}\times\boldsymbol{B}$ drift orbits. The drift motion causes a flow that supplies (extracts) particles to (from) the chaos region. This convection plays an essential role to enable a continuous production of heat in the chaos region.

We study collisionless motion of charged particles governed by Newton's equation with the given fields (1) and (2):

$$m\frac{d\boldsymbol{v}}{dt}=q(\boldsymbol{E}+\boldsymbol{v}\times\boldsymbol{B}), \tag{4}$$

where m and q are the mass and charge, respectively, and $\boldsymbol{v}$ is the velocity of a particle. We normalize variables as

$$\boldsymbol{x}=\ell_x\hat{\boldsymbol{x}},\quad \boldsymbol{B}=B_0\hat{\boldsymbol{B}},\quad t=\tau_A\hat{t},$$

$$\boldsymbol{v}=V_A\hat{\boldsymbol{v}},\quad \boldsymbol{E}=(M_A V_A B_0)\hat{\boldsymbol{E}}, \tag{5}$$

where B_0 is an appropriate measure of the magnetic field, V_A is the Alfvén velocity corresponding to B_0, $\tau_A\equiv\ell_x/V_A$, and M_A is the Alfvén Mach number ($M_A V_A$ gives the $\boldsymbol{E}\times\boldsymbol{B}$-drift convection speed). Using the normalized variables, Eq. (4) reads

$$\frac{\lambda}{\ell_x}\frac{d\hat{\boldsymbol{v}}}{d\hat{t}}=M_A\hat{\boldsymbol{E}}+\hat{\boldsymbol{v}}\times\hat{\boldsymbol{B}}, \tag{6}$$

where $\lambda=V_A/\omega_c$ is the collisionless skin depth and

$$\hat{\boldsymbol{B}}=\begin{cases}(\hat{y}\mp\ell,\hat{x},0) & (|\hat{y}|>\ell)\\ (0,\hat{x},0) & (|\hat{y}|\leqslant\ell),\end{cases} \tag{7}$$

where $\ell\equiv\ell_y/\ell_x$. The left-hand side of Eq. (6) gives the "kinetic effect" that enables deviation from the $\boldsymbol{E}\times\boldsymbol{B}$-drift motion (principal part of the ideal magnetohydrodynamic flow), resulting in chaotic orbits. In what follows, we take $\ell_x=\lambda$ to emphasize the kinetic effect (hence, $\tau_A^{-1}=\omega_c$: cyclotron frequency). If we define ω_c including the sign of the charge (ω_c is positive for ions and negative for electrons), Eq. (6) can be applied for both ions and electrons.

III. SINGLE-PARTICLE DYNAMICS

A. Chaotic orbit

Figure 2 shows two types of orbits projected onto an x-y plane. In Fig. 2(a), we observe that a particle moves irregularly near the Y points while it becomes more regular near the asymptotic line of the magnetic field. Because of the mirror effect of the magnetic field, a particle goes back to the chaos region and is confined there for a certain time. In Fig. 2(b), a larger electric field ($M_A=0.01$) is applied. After a relatively short staying time, the particle escapes from the chaos region.

In Fig. 3, we plot the average staying time ($\hat{\tau}_1\equiv\tau_1/\tau_A$) as a function of M_A. We may approximate $\hat{\tau}_1\approx M_A^{-1}$. This relation does not depend significantly on ℓ as far as $\ell\lesssim 10$. In the limit of $\ell\to\infty$, the magnetic field becomes one dimensional and the orbit becomes integrable.

B. Lyapunov exponents

The maximum Lyapunov exponent of a given orbit characterizes the mean divergence rate of nearby orbits. In a chaotic system, it provides a quantitative measure of the degree of stochasticity. First, we define a quantity to measure divergence of two trajectories in a unit time,

$$\chi(t)\equiv\frac{1}{\Delta t}\ln\frac{|\delta\boldsymbol{x}(t+\Delta t)|}{|\delta\boldsymbol{x}(t)|}, \tag{8}$$

where $\delta\boldsymbol{x}$ is a distance of initially neighboring two trajectories (a basis vector in the most divergent direction). Here we

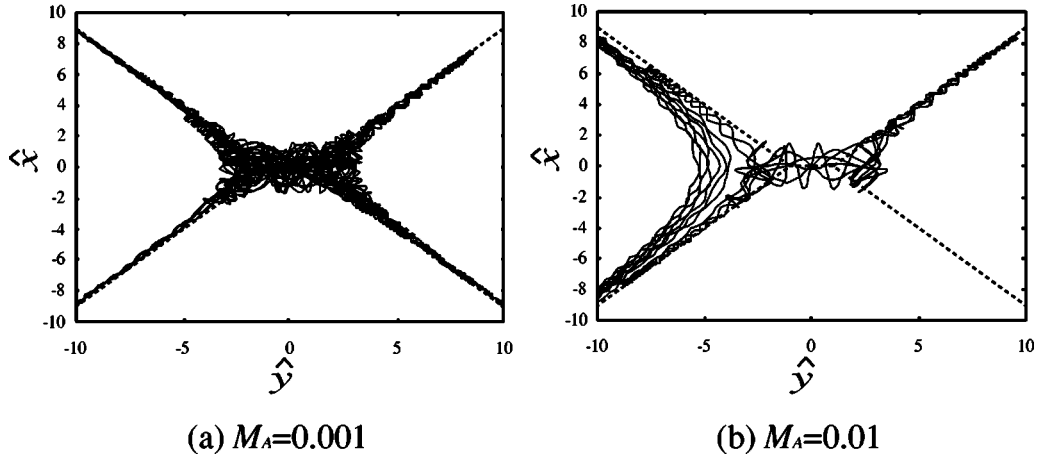

FIG. 2. Typical particle orbit in a Y-shape magnetic field with $\ell=1$. The dotted line shows the asymptotic line of the magnetic field. Motions are qualitatively the same for both figures, however, the staying times are different for different M_A's. In (b), the particle is swept out before it is randomized sufficiently.

set $\Delta t=10^{-2}\tau_A$, $|\delta \mathbf{x}|=10^{-2}\ell_x$. To detect the principal axis of the Hessian, we reorthonormalize the basis vector using the Gram-Schmidt method to find the most rapidly growing direction [8]. The conventional maximum Lyapunov exponent is defined by taking a long-time average of $\chi(t)$ over a certain orbit [7,9]; i.e., choosing sufficiently small Δt and $|\delta \mathbf{x}|$, one may calculate

$$\overline{\chi} \equiv \lim_{N\to\infty} \frac{1}{N\Delta t} \sum_{n=0}^{N} \chi(t_n)\Delta t. \tag{9}$$

However, this definition is not suitable when we consider an open system where the particle staying time is finite. To quantify the degree of stochasticity for a temporally and spatially finite chaotic phase of motion, we take an ensemble average, instead of the long-time average, to define a temporally and spatially local maximum Lyapunov exponent (LLE) [10]:

$$\tilde{\chi}(t) \equiv \langle \chi(t) \rangle. \tag{10}$$

The ensemble average $\langle \cdot \rangle$ is taken for the particles contained in a given region defined as follows: Particles are initially distributed uniformly in the region $-1.0<\hat{x},\hat{y}<1.0$ and $-0.5<\hat{v}_x,\hat{v}_y,\hat{v}_z<0.5$ (total number is 5×10^4). We consider subdomains $\Omega(R)$ scaled by the distance from the Y points; $R\equiv\sqrt{\hat{x}^2+(\hat{y}-\ell)^2}$. To measure the strength of chaos near the Y points, we evaluate LLE for the ensemble of particles remaining in $\Omega(R)$. In Fig. 4, we plot LLEs [for different $\Omega(R)$] as functions of $\hat{t}$. For larger R ($R\gtrsim1$), the LLE decreases as $\hat{t}$ increases, simply that $\Omega(R)$ contains regions where particle motion becomes regular. A stationary value of LLE is observed for $R\lesssim1$. Hence, we may call $\Omega(1)$ the chaos region where the LLE is about 0.25.

In Fig. 5, we compare the LLEs for different M_A's (and hence, for different staying times). For $M_A<0.01$, the LLEs have a plateau at the same level (LLE$\simeq$0.25). When M_A

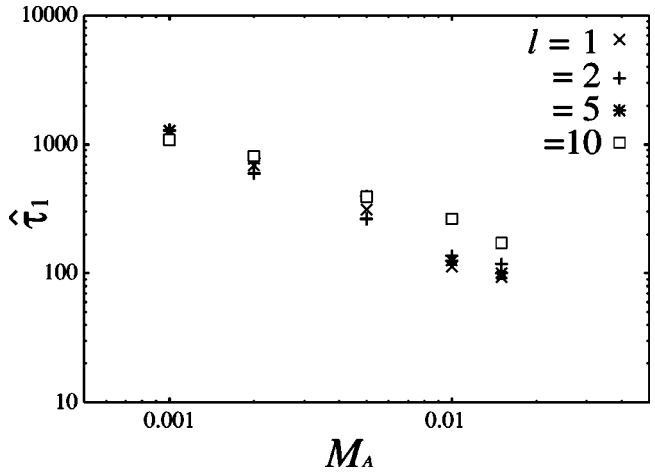

FIG. 3. Average staying time in the chaos region ($\hat{\tau}_1$) as a function of M_A.

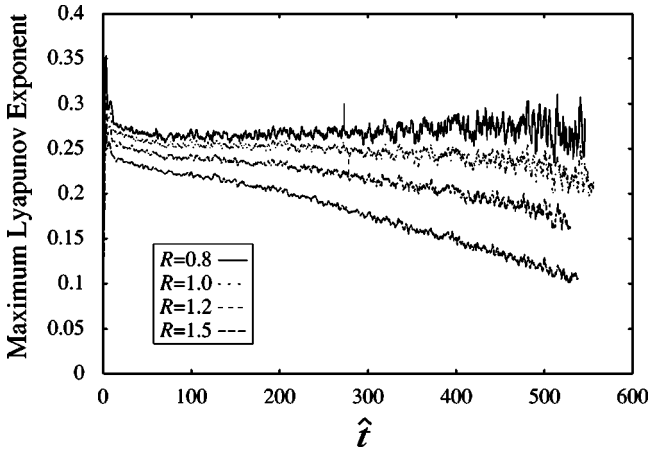

FIG. 4. Local Lyapunov exponents for different subdomains $\Omega(R)$ ($M_A=0.002$). We define the chaos region such that the local Lyapunov exponents have a plateau ($R\lesssim1.0$).

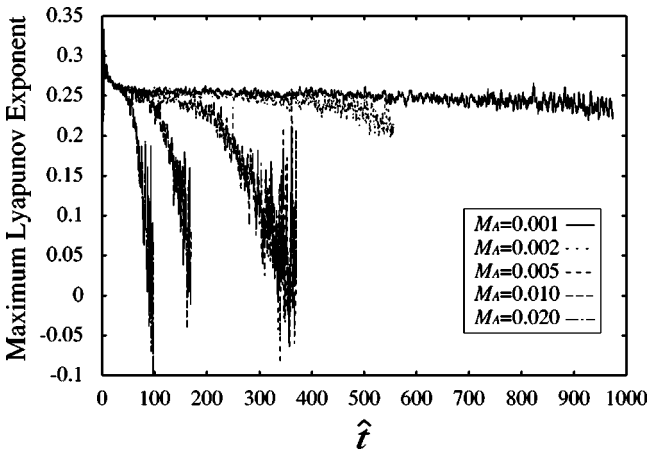

FIG. 5. Local Lyapunov exponents for different M_A's. For larger M_A, the local Lyapunov exponents are strongly damped and have no plateau region.

$\gtrsim 0.01$, however, the plateau is lost because all particles are swept out from the chaos region before they are randomized.

IV. STATISTICAL DISTRIBUTION AND MACROSCOPIC RESISTIVITY

A. Velocity distribution

Macroscopic quantities, such as temperature and resistivity, are calculated invoking many particles that obey the same equation of motion with random initial conditions; initial velocities and positions have a uniform distribution in the domain of $-0.5<\hat{v}_x,\hat{v}_y,\hat{v}_z<0.5$ and $-1.0<\hat{x},\hat{y}<1.0$. In Figs. 6(a)–6(c), we plot the velocity distributions of the particles in the chaos region $\Omega(1)$ with the Gaussian fitting curves. In the initial phase ($\hat{t}\sim\tilde{\chi}^{-1}\simeq 4$), particles relax into almost isotropic Gaussian distributions. Temporal evolutions of the distributions are shown in Figs. 6(d)–6(f). The total number of particles decreases because of the loss of particles from the chaos region. The peak of distribution of $\hat{v}_z$ gradually shifts in the direction of the electric field. The velocity distributions have cut off around $|v|\sim 0.8$, implying that particles with $|v|\gtrsim 0.8$ are lost from the chaos region. Indeed, if $|v|\gtrsim 0.8$, the particle passes the chaos region in a unit time and such a high energy particle cannot be scattered by the Y points.

Figure 7 shows the standard deviations (temperatures) of the velocity distributions. We observe that the temperatures increase in the x and y directions. In the direction of the electric field (z direction), particles have an average flow velocity. The distribution is strongly distorted in the $\hat{v}_z\gtrsim 1$ region, and the standard deviation decreases.

B. Effective resistivity

We may estimate the effective collisionless resistivity from the evolution of the average velocity in the direction of the electric field (Fig. 8). The ensemble average is taken over the particles in the chaos region $\Omega(1)$. Particles in the chaos region are accelerated monotonically; we may write

$$\overleftarrow{v_z}(\hat{t})\simeq\alpha\hat{t}$$

with

$$\alpha=3.48\times10^{-4}. \tag{11}$$

However, the number of particles in the chaos region decreases exponentially (Fig. 9):

$$n(\hat{t})\simeq n_0\exp(-\beta\hat{t})$$

with

$$\beta=2.17\times10^{-3}. \tag{12}$$

We may consider a system where the total number of particles is conserved with supplying particles with zero average velocity; this model is more appropriate to simulate a convecting system with a driving electric field. Using Eqs. (11) and (12), we obtain the average velocity in such a sustained system:

$$\overleftarrow{v_w}(\hat{t})=\frac{\alpha}{\beta}[1-\exp(-\beta\hat{t})]. \tag{13}$$

The macroscopic velocity may be modeled by a dissipative evolution equation

$$\hat{\rho}_{\rm eff}\frac{d\overleftarrow{v_z}}{d\hat{t}}=M_A\hat{E}-\hat{\nu}_{\rm eff}\overleftarrow{v_z}, \tag{14}$$

where $\overleftarrow{v_z}$ is the normalized average velocity in the z direction, $\hat{\rho}_{\rm eff}$ is the effective mass normalized by the particle mass, and $\hat{\nu}_{\rm eff}$ is an effective collision frequency normalized by ω_c. To explain the meaning of the effective mass, let us first assume $\hat{\rho}_{\rm eff}=1$. Then, the solution of Eq. (14) becomes

$$\overleftarrow{v_z}=\frac{M_A\hat{E}}{\hat{\nu}_{\rm eff}}[1-\exp(-\hat{\nu}_{\rm eff}\hat{t})]. \tag{15}$$

Evaluating $\hat{\nu}_{\rm eff}$ from the time constant of the numerical result [see Eq. (13)], we obtain the saturation level of the velocity

$$\overleftarrow{v_{\rm sat}}=\frac{M_A\hat{E}}{\hat{\nu}_{\rm eff}}, \tag{16}$$

which translates as $E/(V_AB_0)=\hat{\nu}_{\rm eff}(\overline{v_{\rm sat}}/V_A)$ in the physical units. Comparing this relation with Ohm's law (j is the current density, n is the number density, q is the electric charge)

$$E=\eta_{\rm eff}j=\eta_{\rm eff}nq\overline{v_{\rm sat}}, \tag{17}$$

we obtain

$$\frac{\eta_{\rm eff,1}}{\mu_0}=\lambda^2\omega_c\hat{\nu}_{\rm eff}. \tag{18}$$

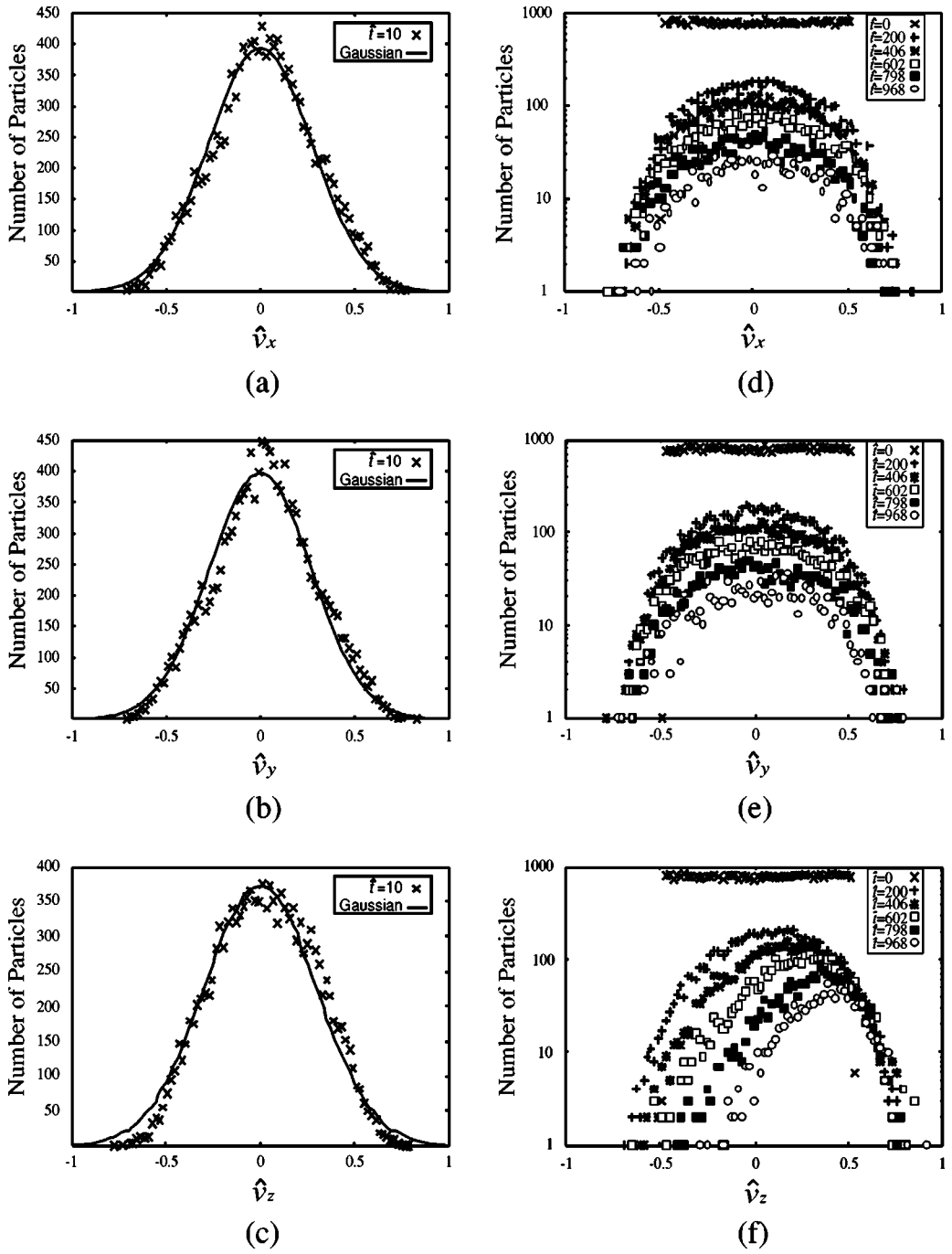

FIG. 6. Velocity distributions in the chaos region ($M_A=0.001, \ell=0$). (a)–(c): distributions of v_x, v_y, v_z, after initial randomization phase with the Gaussian fitting curves. (d)–(f) Temporal evolutions of the distributions of v_x, v_y, v_z.

We can derive another resistivity directly from the saturation level. By substituting the value of $\hat{v}_{\mathrm{sat}}$ into Eq. (17), we obtain

$$\frac{\eta_{\mathrm{eff},2}}{\mu_0}=\lambda^2\omega_c\frac{M_A\hat{E}}{\hat{v}_{\mathrm{sat}}}. \tag{19}$$

These two resistivities ($\eta_{\mathrm{eff},1}$ and $\eta_{\mathrm{eff},2}$) do not agree, because Eq. (14) is a phenomenological model—the microscopic magnetic force $q\boldsymbol{v}\times\boldsymbol{B}$ is absorbed both in the frictional and inertia terms in the averaged (macroscopic) model. By adjusting the mass to $\hat{\rho}_{\mathrm{eff}}$ in the inertia term of Eq. (14), the solution of Eq. (14) modifies as

$$\hat{v}_z=\frac{M_A\hat{E}}{\hat{\nu}_{\mathrm{eff}}}\left[1-\exp\left(-\frac{\hat{\nu}_{\mathrm{eff}}}{\hat{\rho}_{\mathrm{eff}}}\hat{t}\right)\right]. \tag{20}$$

By plugging Eqs. (13) and (20), we obtain $\hat{\nu}_{\mathrm{eff}}=6.2\times10^{-3}, \hat{\rho}_{\mathrm{eff}}=2.9$. The effective resistivity is given by (in physical units)

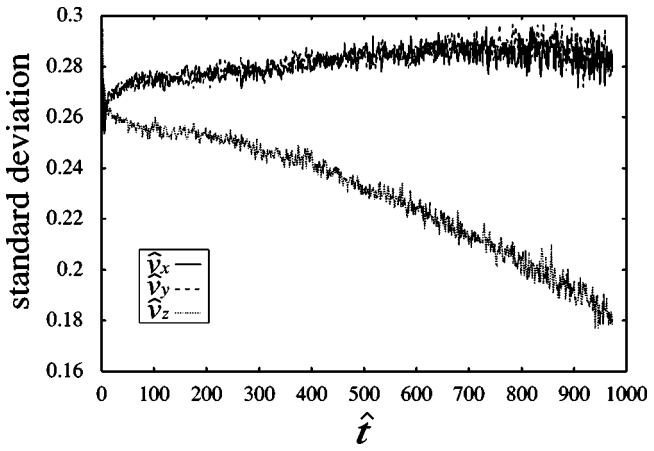

FIG. 7. Standard deviations of the velocity distribution ($M_A = 0.001, \ell = 0$).

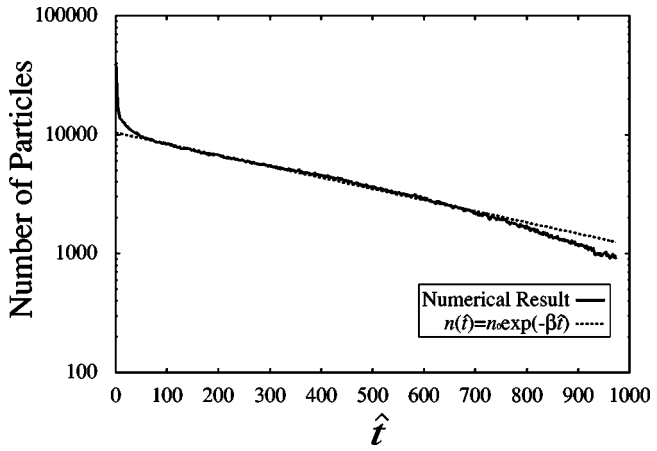

FIG. 9. Evolution of the number of particles in the chaos region. The number decreases exponentially.

$$\frac{\eta_{\rm eff}}{\mu_0} = \lambda^2 \omega_c^2 \nu_{\rm eff}. \tag{21}$$

V. SUMMARY

Chaotic motion of particles in strongly inhomogeneous magnetic fields is a simple and direct route to produce a collisionless resistivity. In magnetic null regions, particles are unmagnetized and describe extremely complex orbits, which invalidates theoretical models based on wave-particle interactions [4] or stochastic motion of magnetized fluids [5].

In an inhomogeneous magnetic field, charged particles describe chaotic orbits. The randomization of the phase of cyclotron motion enables particles to receive net acceleration from the electric field. The phenomenological dissipation equation is introduced to evaluate a current parallel to the electric field. In a macroscopic model (14), the chaotic randomization effect [$\boldsymbol{v}\times\boldsymbol{B}$ term in the particle model (4)] is described by both the effective collision frequency and the effective mass. The effective collision frequency only is not sufficient to account for the chaos effect. From the effective collision frequency, we obtain a collisionless effective resistivity. In the absence of mutual interactions among particles, we may construct a stationary state by supplying new particles that are just replicas of particles with shifted initial times. The velocity distributions of particles broaden and achieve almost isotropic Gaussian distribution. The average staying time of particles in the chaos region, relative to the maximum LLE, is the key parameter that restricts the maximum electric field (or the Mach number) to yield an appreciable resistivity—too large electric field sweeps out particles from the chaos region before they are randomized.

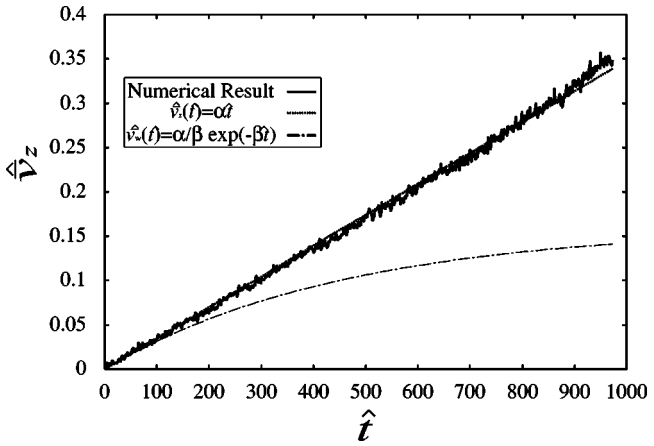

FIG. 8. Evolution of the average velocity in the direction of the electric field ($M_A = 0.001$, $\ell = 0$). The ensemble consists of the particles remaining in the chaos region. The average velocity increases linearly. The dotted line shows a linear fitting curve. The dot-dashed line shows the average velocity weighted by the number of particles (13).

The "chaos-induced resistivity" is proportional to the square of the Alfvén velocity ($V_A = \lambda\omega_c$), which is a function of the magnetic field and the plasma density. On the other hand, the classical collisional resistivity (Spitzer resistivity [11]) is a function of the electron temperature ($\propto T_e^{-3/2}$). In a high temperature plasma, the chaos-induced resistivity ($\eta_{\rm eff}$) can be much larger than the classical collisional resistivity. For example, if we take typical parameters of the solar corona ($n = 10^{16}\ {\rm m}^{-3}$, $B_0 = 10^{-2}$ T, $T_e = 10^2$ eV), $\eta_{\rm eff}$ is about 10^4 times larger than the collisional resistivity. The chaos-induced resistivity occurs both in ions and electrons. Ions contribute much larger dissipation than electrons, because the size of the ion chaos region (scaled by the skin depth) is much larger than that of electrons. This chaos-induced resistivity has been applied to explain the fast (shock-type) reconnection process. Introducing a mesoscopic model in the diffusion region [6,12], we may avoid the unphysical scale reduction problem that Petschek's model [13] encountered. The bound for the Mach number restricting this collisionless resistivity explains the time scale of the fast reconnection.

ACKNOWLEDGMENTS

This work was supported by Toray Science Foundation and a Grant-in-Aid for Scientific Research from the Japanese Ministry of Education, Science, and Culture, Grant No. 14802033.

[1] J. Egedal and A. Fasoli, Phys. Rev. Lett. **86**, 5047 (2001).
[2] W. Horton *et al.*, Phys. Fluids B **3**, 2192 (1991); W. Horton *et al.*, Geophys. Res. Lett. **18**, 1575 (1991).
[3] Z. Yoshida *et al.*, Phys. Rev. Lett. **81**, 2458 (1998).
[4] J.F. Drake and T.T. Lee, Phys. Fluids **24**, 1115 (1981).
[5] A.H. Boozer, J. Plasma Phys. **35**, 133 (1986); P.K. Kaw *et al.*, Phys. Rev. Lett. **43**, 1398 (1979); T.H. Stix, Nucl. Fusion **18**, 353 (1978).
[6] R. Numata and Z. Yoshida, Phys. Rev. Lett. **88**, 45003 (2002).
[7] A.J. Lichtenberg and M.A. Lieberman, *Regular and Chaotic Dynamics* (Springer-Verlag, New York, 1992).
[8] I. Shimada and T. Nagashima, Prog. Theor. Phys. **61**, 1605 (1979).
[9] G. Benettin *et al.*, Phys. Rev. A **14**, 2338 (1976).
[10] C. Beck and F. Schlögl, *Thermodynamics of Chaotic Systems, an Introduction* (Cambridge University Press, Cambridge, 1993), pp. 158–177.
[11] L. Spitzer, *Physics of Fully Ionized Gases* (Interscience, New York, 1956).
[12] S.M. Mahajan and Z. Yoshida, Phys. Rev. Lett. **81**, 4863 (1998); Z. Yoshida *et al.*, Phys. Plasmas **8**, 2125 (2001).
[13] H.E. Petschek, in *AAS-NASA Symposium on Physics of Solar Flares*, edited by W.N. Hess (National Aeronautics and Space Administration, Washington, D.C., 1964), SP-50.